Supplementary Materials for

Zinc-Alcohol-Air Batteries with Ultra-Narrow Cyclic Voltage Windows

Zilong Li[†, a, b], Shunlian Ning[†, c], Yanshuo Jin[a], Nan Wang*[, a], Shuhui Sun*[, d], Hui Meng*[, a]

[a]Siyuan Laboratory, Guangzhou Key Laboratory of Vacuum Coating Technologies and New Energy Materials, Guangdong Provincial Engineering Technology Research Center of Vacuum Coating Technologies and New Energy Materials, Guangdong Provincial Key Laboratory of Nanophotonic Manipulation, Department of Physics, Jinan University, Guangzhou, Guangdong 510632, China

*Emails: nanwang@jnu.edu.cn (N.W.); tmh@jnu.edu.cn (H.M.)

[b]School of Chemistry and Materials Science, University of Science and Technology of China, Hefei, Anhui 230026, China

[c]School of Chemistry, Sun Yat-Sen University, Guangzhou, Guangdong 510275, China

[d]Institut National de la Recherche Scientifique (INRS), Center Énergie Matériaux Télécommunications, Varennes, Québec J3X 1P7, Canada

* E-mail: shuhui.sun@inrs.ca (S. Sun)

†These authors contributed equally to this work.

The PDF file includes:

Materials and Methods

Chemicals

$HAuCl_4 \cdot 3H_2O$ (99.9%), $PdCl_2$ (98%), $H_2PtCl_6 \cdot 6H_2O$ (AR), $NaBH_4$ (98%), polyvinyl alcohol (PVA, 98% alcoholysis), zinc acetate dihydrate ($Zn(Ac)_2$, 99.99%), ethylene glycol (EG, 99%), glycerin (Gly, 99%) and deuteroxide (D_2O, 99.99%) were purchased from Aladdin. Ethanol (EtOH, 99.7%), erythritol (Ery, 99%), potassium hydroxide (KOH, 95%) and acetic acid (99.99%) were purchased from Macklin. Ketjen Black (ECP-600JD) was purchased from LION. The carbon cloth coated with gas diffusion layer (W1S 1009) was purchased from CeTech. The high purity zinc plates (0.4 mm, 99.999%) and Ni foam (1 nm, 99.99%) were purchased from High Purity Metal Materials Research Institute on *Taobao.com*. All water was ultra-pure water from the HITECH system (18.2 MΩ).

Materials Synthesis

Before production, the solutions of noble metals and freshly reductant need to be prepared. First, 1 g $HAuCl_4 \cdot 3H_2O$ and $H_2PtCl_6 \cdot 6H_2O$ were dissolved in 100 mL deionized water (DIW), respectively. And 1 g $PdCl_2$ was dissolved in 100 mL 0.5 M HCl solution. Then, all three solutions were transferred to brown reagent bottles respectively and stored in the refrigerator at 5 °C. The 0.2 M $NaBH_4$ solution must be prepared before each synthesis and used as soon as possible.

The model catalyst was synthesized by sol immobilization. Typically, 4 mL $HAuCl_4$ solution and 2 mL $PdCl_2$ solution were added to 300 mL DIW and stirred evenly. Then, PVA of the same actual mass as the noble metal (Au and Pd) was directly mixed and dissolved in the solution by 10 min magnetic stirring. Freshly reductant solution (0.2 M $NaBH_4$, $NaBH_4$/metal = 5/1, mole/mole) was added to the solution quickly and further formed a colloidal solution. After that, 318 mg carbon support (Ketjen Black) was added to the colloidal solution. The mixture was stirred for 30 min and allowed to age for 10 min naturally. The speed of magnetic stirring in the experiment is 600 rpm. Finally, the product was obtained by suction filtration, washed with 1 L DIW and dried at 115 °C for 1 h. The as-synthesized material was named AuPd@C. For comparison, the Au@C, Pd@C and Pt@C model catalysts were also synthesized by only adding 4 mL $HAuCl_4$ solution, 4 mL $PdCl_2$ solution and 4 mL H_2PtCl_6 solution in the initial step, respectively.

Battery Assembly

Zinc-alcohol-air batteries and traditional zinc-air batteries were assembled using a polished 0.4 mm Zn plate as the negative electrode, catalyst-loaded carbon cloth (with a gas diffusion layer) as the positive electrode, and a 6.0 M KOH with 0.1 M $Zn(Ac)_2$ (with alcohol) as electrolyte. To prepare the gas diffusion electrode, 5.0 mg of composite catalyst powder was dispersed in 980 μL ethanol and mixed with 20 μL of 5 wt% Nafion solution. The mixture was sonicated for 30 min to form a homogeneous catalyst ink. The catalyst ink was then uniformly sprayed onto a pre-cleaned hydrophobic carbon cloth with a gas diffusion layer to obtain a metal (Au, Pd or Pt) mass loading of 0.1 mg cm^{-2}. The effective area of both the positive and negative electrodes was a 1.0 cm^2 circular region. The initial alcohol concentration in the electrolytes of zinc-alcohol-air batteries was set to provide a 1.0 M hydroxyl group ([-OH]) concentration. The alcohol concentrations in the electrolytes were 1.0 M ethanol, 0.5 M glycol, 0.33 M glycerin, and 0.25 M erythritol. Each battery contained 4 mL of electrolyte. During cyclic tests, the electrolytes of zinc-alcohol-air batteries were refreshed every 20 h to maintain the alcohol concentration. All tests were conducted at room temperature in an air or oxygen controlled environment.

.

Characterization

The phase composition was identified by X-ray diffraction (XRD) using the Miniflex600 diffractometer (Cu Kα, λ=1.54056 Å radiation). The High-Resolution Transmission Electron Microscope (HRTEM, JEOL 2100F) and scanning transmission electron microscope (STEM) were applied to characterize the morphology and structure of the catalysts. The chemical composition was measured by X-ray photoelectron spectroscopy (XPS, ESCALAB 250, Mg Kα) and inductively coupled plasma-mass spectrometry (ICP, OPTIMA 2000DV). The Nuclear Magnetic Resonance Spectroscopy (NMR, Bruker Ascend 500 M & 600 M) was conducted for qualitative and quantitative analysis of reaction products.

Electrochemistry

A three-electrode system with the electrochemical workstation (SP-150, Bio-Logics) was applied to the electrochemical measurements for alcohol oxidation reactions (AOR). AOR measurements used the same electrolyte (6 M KOH with alcohol) and collector as the battery to simulate the actual application scenario as much as possible. Carbon clothes (1.0×1.0 cm^2) loaded with an as-prepared catalyst were used as the working electrodes. A carbon rod and saturated

Hg/HgO electrode functioned as counter and reference electrodes, respectively. To prepare the working electrode, 5.0 mg of composite catalyst powder was dispersed in 980 μL ethanol and contained with 20 μL of 5 wt% Nafion solution, and the mixture was sonicated for 30 min to form a homogeneous catalyst ink. The ink was dropped onto the carbon cloth electrode at the metal loading of 0.100 mg cm^{-2} and dried at room temperature. The Hg/HgO reference electrode was calibrated with respect to a reversible hydrogen electrode (RHE).

The electrochemical measurements for oxygen reduction reaction (ORR) were studied with the three-electrode system on the electrochemical workstations (SP-150 Bio-Logics & AFCBP1 PINE). Since ORR is limited by mass transfer resistance, standard tests (0.1 M KOH, 1600 rpm) are used to evaluate catalyst performance. A glassy carbon electrode was used as the working electrode. Oxygen was bubbled through the electrolyte for 30 min before the start of the ORR testing. Other conditions are consistent with the AOR test condition above. The ORR polarization curves shown in this paper deduct the effects of the electric double layer.

All tests were carried out at 25 °C. Linear sweep voltammograms (LSV) tests were performed at a sweep rate of 10 mV s^{-1}. The polarization curves of AORs were iR-corrected according to the equation: $E_c = E_m - I \times R_s$ (E_c is the corrected potential, E_m is the measured potential experimentally, and R_s is the resistance from the electrolyte/contact resistance measured by EIS). The Faradic efficiency (FE) of $4e^-$ EOR is calculated using the following equation: $FE = (4 \times N_A \times e \times n)/Q \times 100\ \%$ (N_A is Avogadro constant, e is the elementary charge, Q is the total passed charge). The round-trip efficiency (RTE) of the battery is analyzed by the equation: $RTE = (E_{cd}/E_{cc}) \times 100\ \%$ (E are the cut-off potentials of charge and discharge).

Computational Methods

DFT calculations were performed with the CASTEP code of the Materials Studio package from Acclerys Inc. In all calculations, the generalized gradient approximation and the projector augments wave pseudopotentials with the exchange and correlation in the Perdew-Burke-Ernzerh of were employed. The plane-wave cutoff energy and k-point were set to “fine”. The convergence of forces and energy on each atom during structure relaxation was set to 0.03 eV $Å^{-1}$ in force and 10^{-5} eV in energy, respectively. The unit cells of Au, Pd, Pt, and AuPd were in the Fm-3m symmetry groups, respectively. For computing the ethanol, thylene glycol, glycerin, Erythritol adsorption energy and formic acid and acetic acid desorption energy, the four-layer (111) and (200) planes were cleaved as the active surfaces for pure Au, pure Pd, pure Pt and pure AuPd,

respectively. The vacuum space along the z direction was more than 15 Å, which is large enough to avoid interplanar interactions. For geometry optimizations of all slab models, the top two layers were allowed to relax.

The adsorption energies were calculated by $\Delta E_{ads} = E_{ads+sur} - (E_{ads} + E_{sur})$, where $E_{ads+sur}$ represents the total energy of the adsorbate interacting with the surface, E_{ads} is the energy of the adsorbate in the gas phase, and E_{sur} is the energy of the bare surface. The desorption energies were calculated by $\Delta E_{des} = (E_{des} + E_{sur}) - E_{des}+_{sur}$, where $E_{des+sur}$ represents the total energy of the adsorbate interacting with the surface, E_{des} is the energy of the adsorbate in the gas phase, and E_{sur} is the energy of the bare surface.

Supplementary Figures

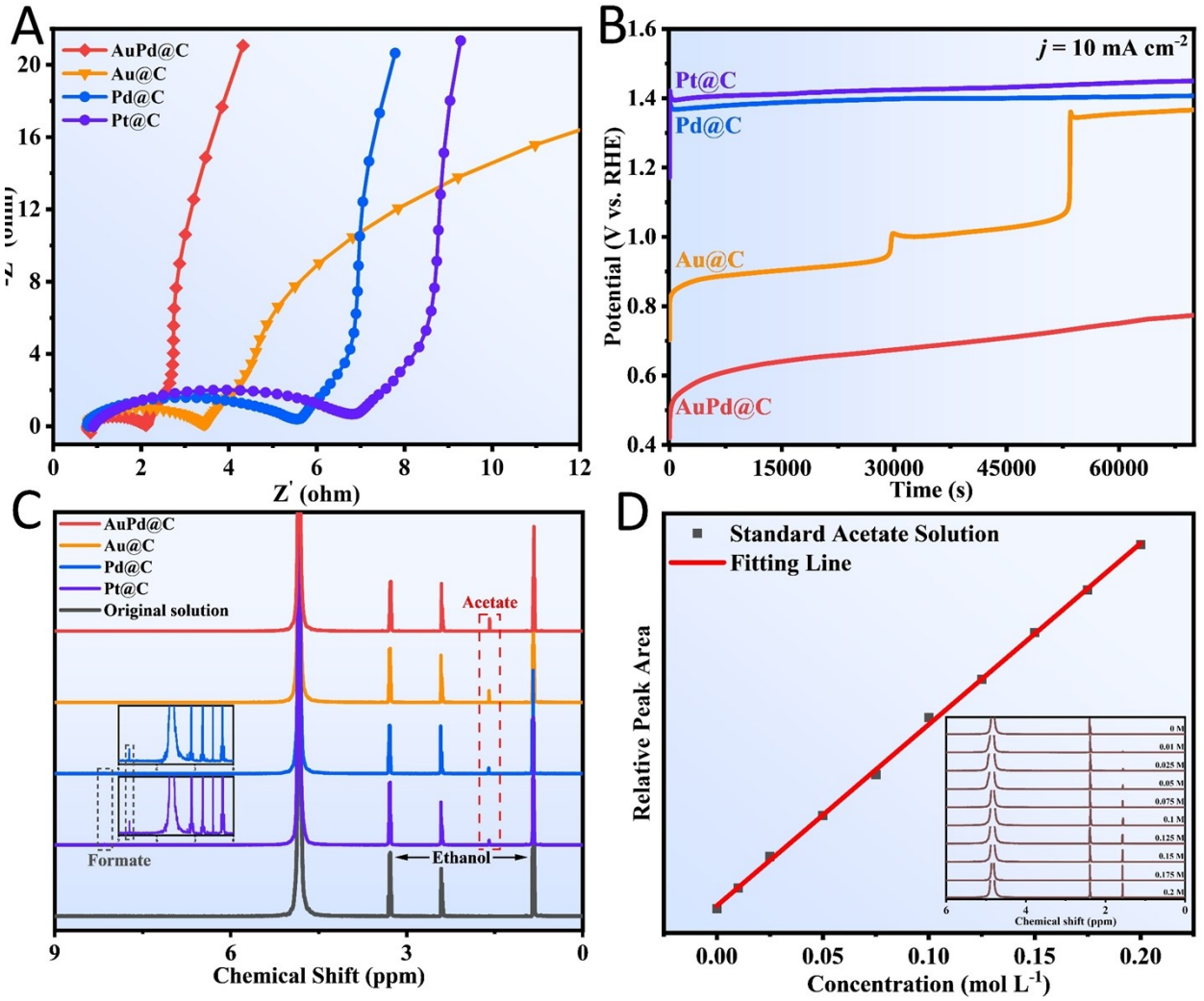

Fig. S1. (A) Nyquist plots and (B) chronopotentiometry stability curves of Au@C, Pd@C, Pt@C and AuPd@C. (C) ^{1}H nuclear magnetic resonance (NMR) spectra of products before and after 72000 s anodic ethanol oxidation on AuPd@C, Au@C, Pd@C and Pt@C electrodes, respectively. (D) Standard curve of acetic acid concentration measured by ^{1}H NMR for Faradaic efficiency analysis.

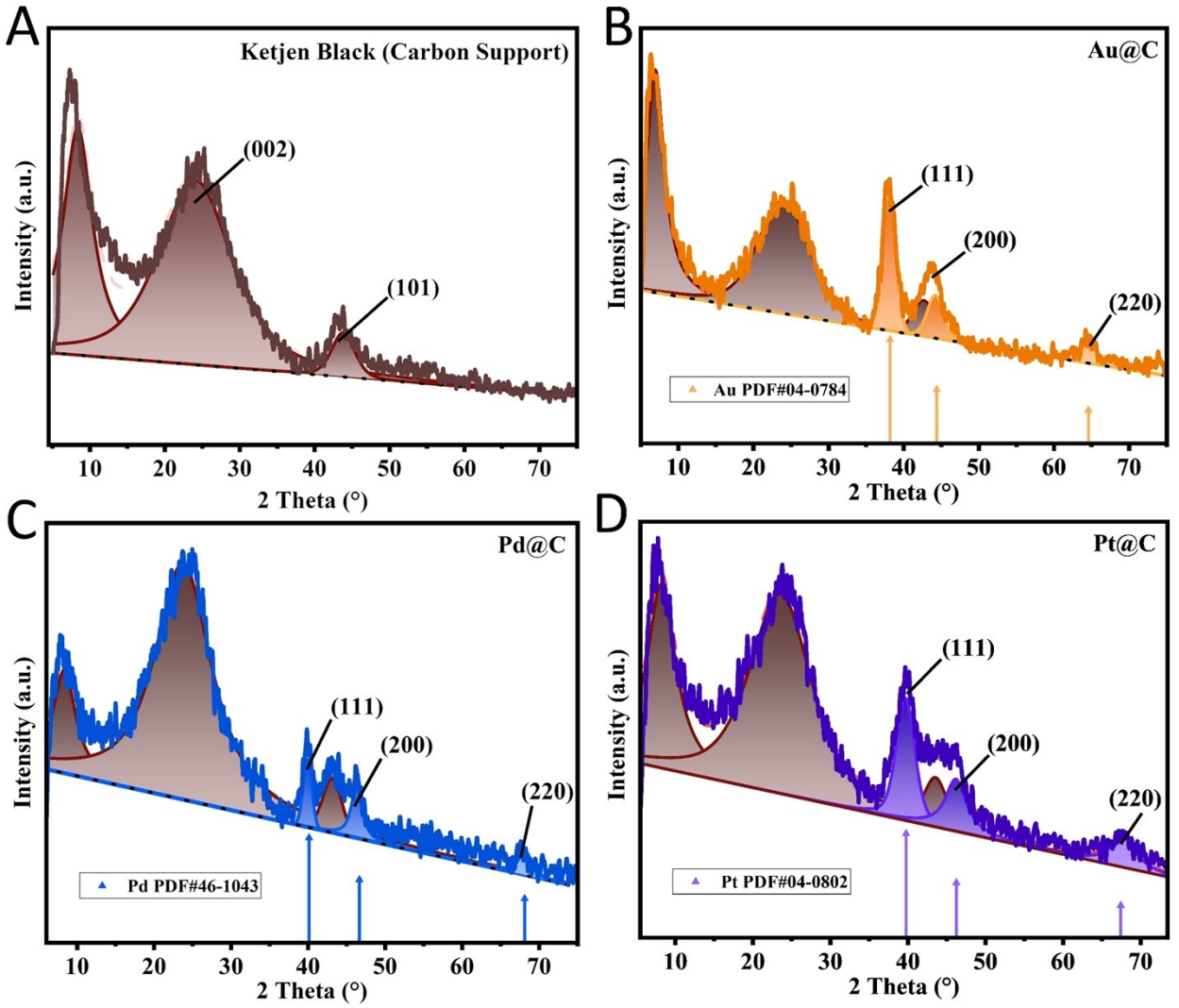

Fig. S2. (A-D) X-ray diffraction pattern of Ketjen Black (carbon support), Au@C, Pd@C and Pt@C, respectively.

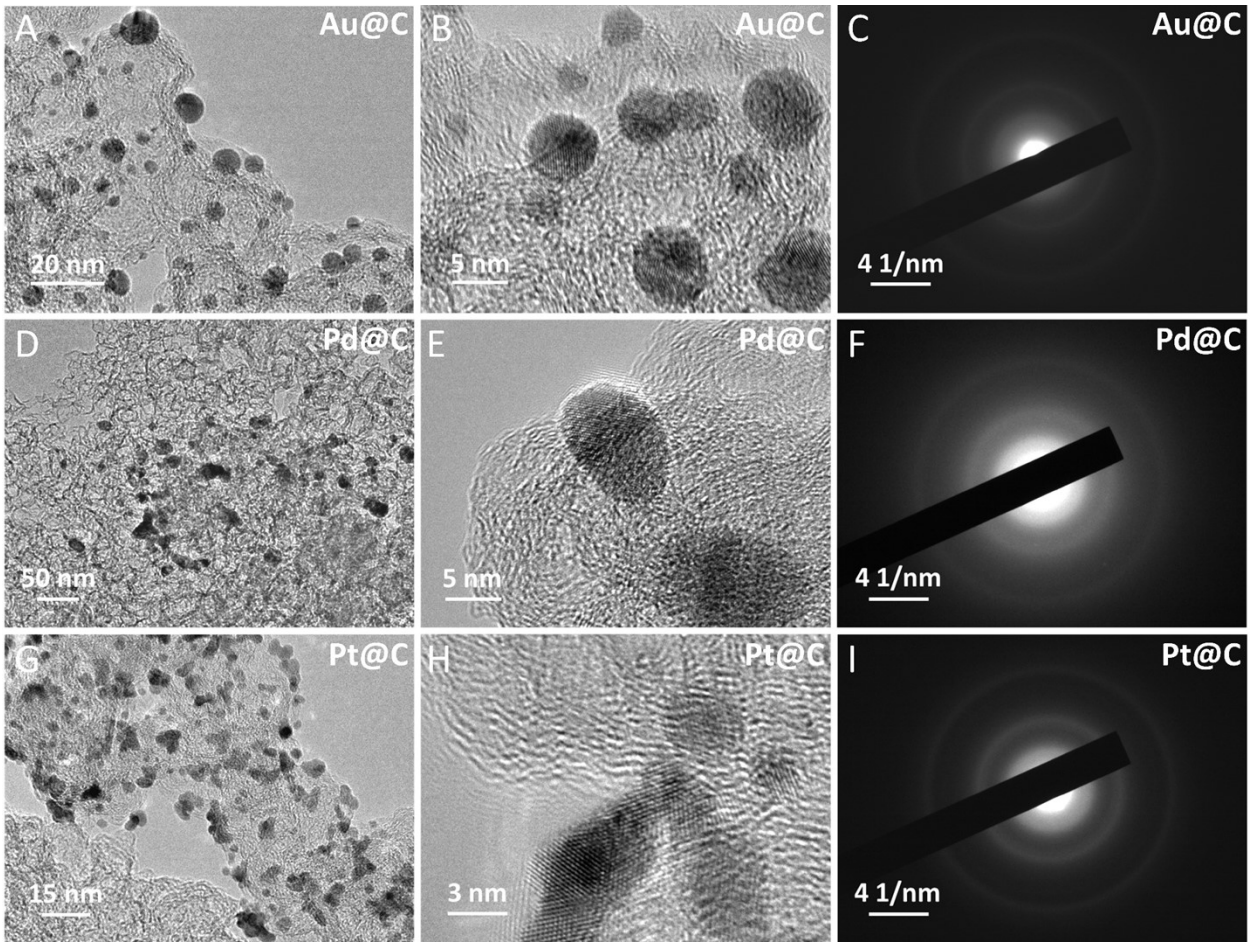

Fig. S3. (A) Transmission electron microscope (TEM) image, (B) high-resolution TEM (HRTEM) image and (C) selected area electron diffraction (SAED) pattern of Au@C. (D) TEM image, (E) HRTEM image and (F) SAED pattern of Pd@C. (G) TEM image, (H) HRTEM image and (I) SAED pattern of Pt@C.

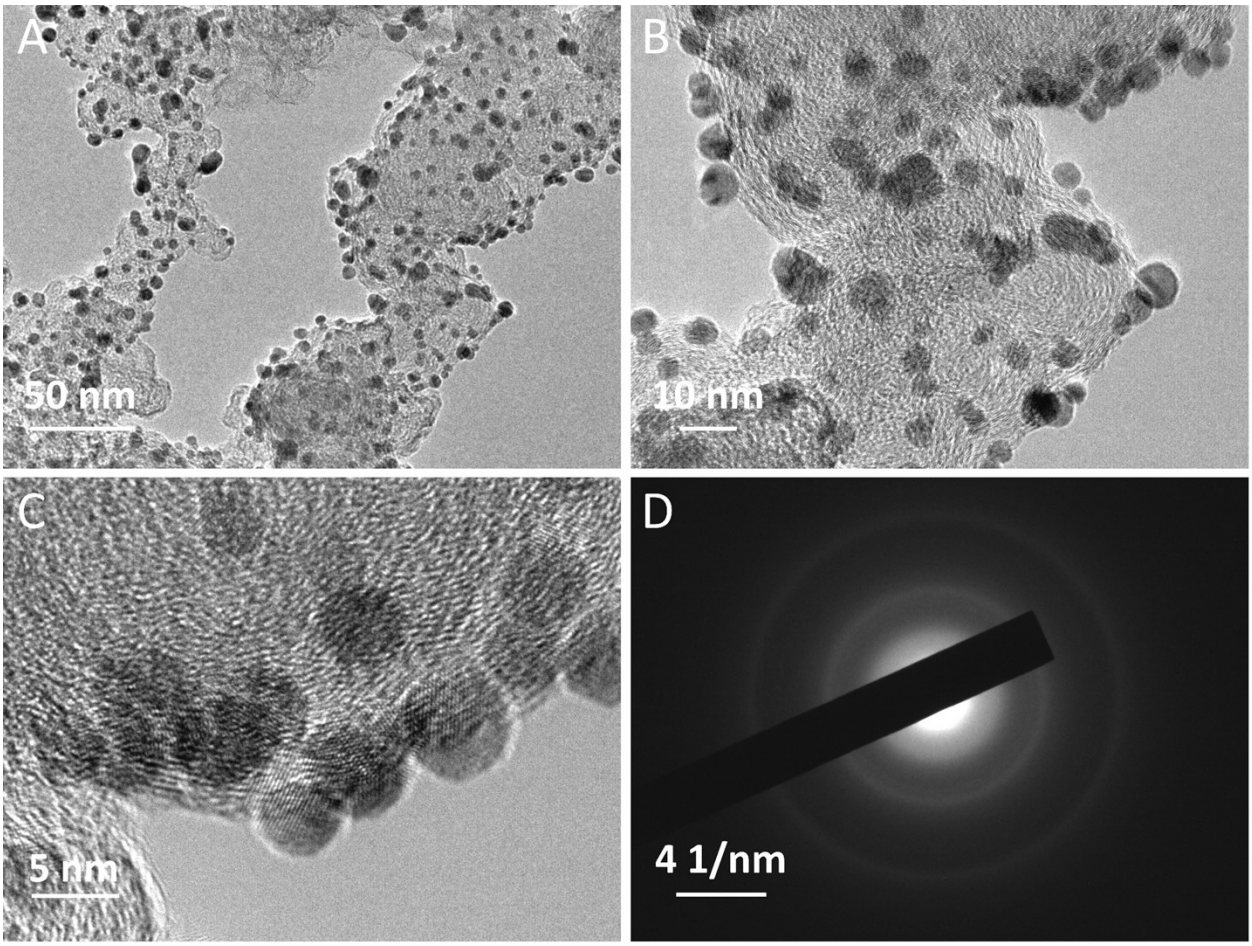

Fig. S4. (A, B) TEM image, (C) HRTEM image and (D) SAED pattern of AuPd@C.

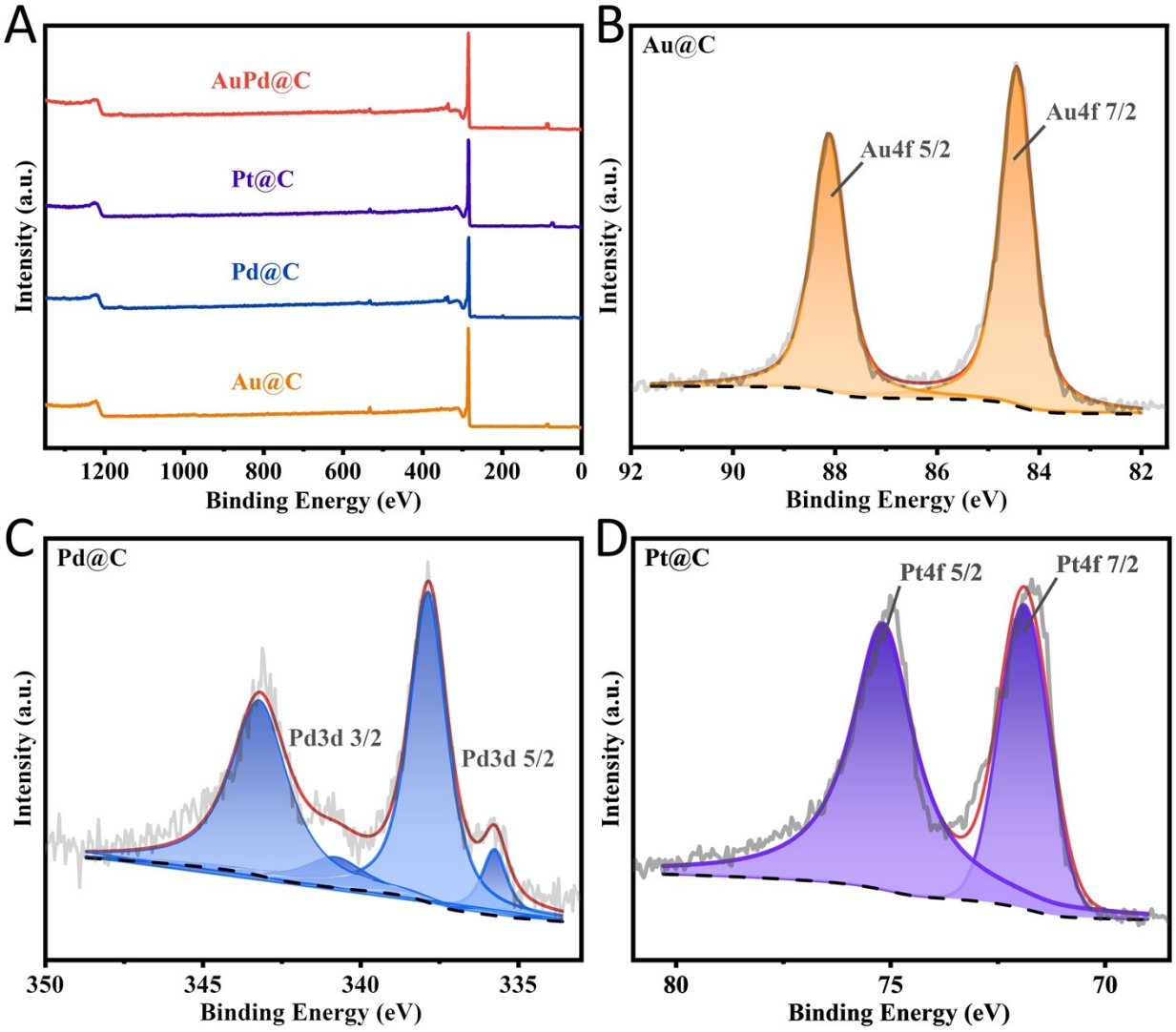

Fig. S5. (A) Wide-scan X-ray photoelectron spectra (XPS) of Au@C, Pd@C, Pt@C and AuPd@C. (B) High-resolution XPS (HRXPS) for Au4f of Au@C. (C) HRXPS for Pd3d of Pd@C. (D)HRXPS for Pt4f of Pt@C.

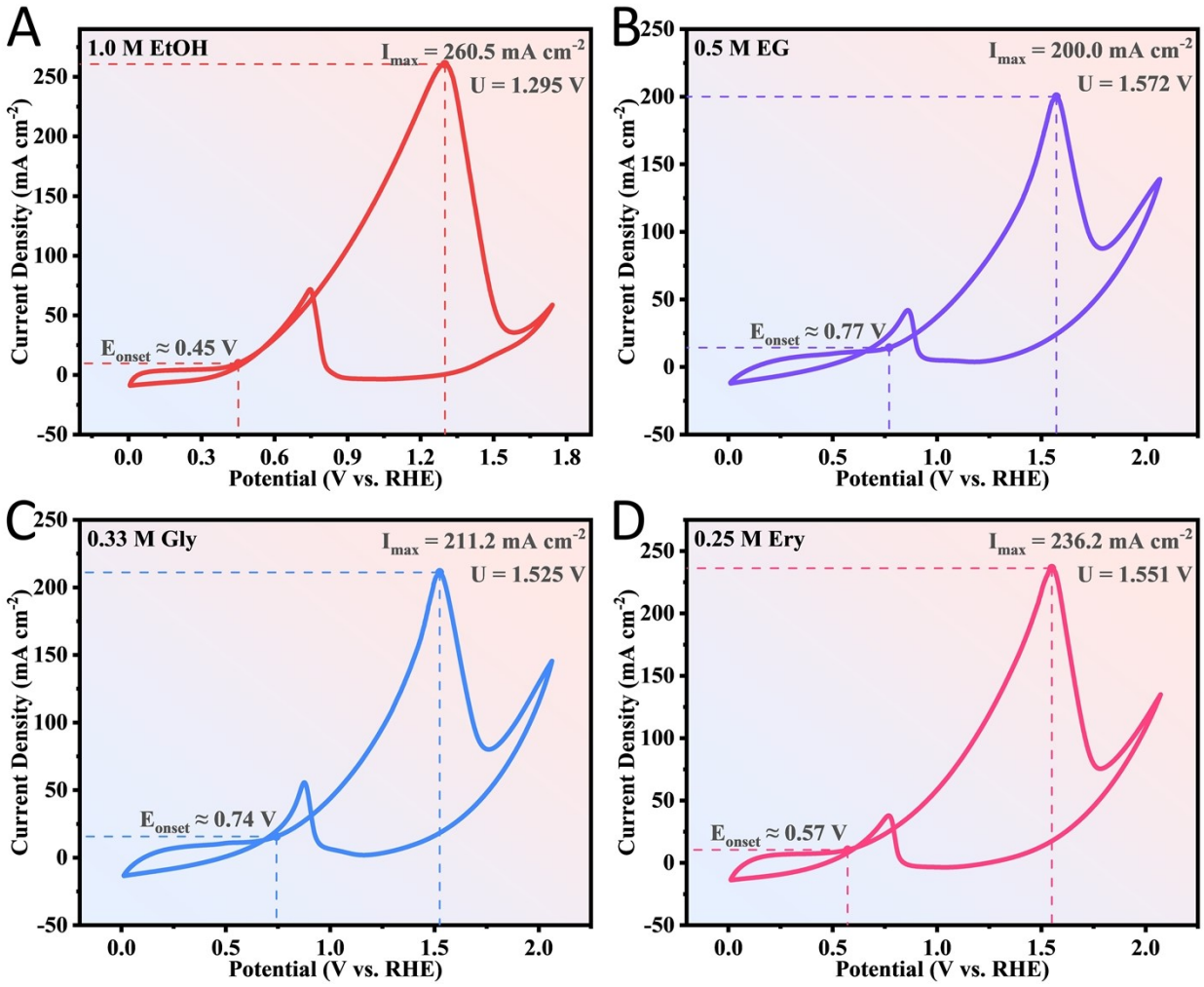

Fig. S6. (A-D) Cyclic voltammetry curves of AuPd@C model catalyst for the organic oxidation reaction of ethanol, glycol, glycerin and erythritol, respectively.

* represent adsorbate	Ethanol	Glycol	Glycerin	Erythritol	Formic Acid	Acetic Acid
Au*Pd@C (111)	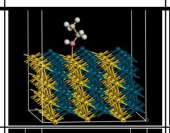	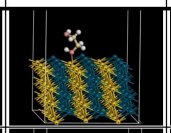	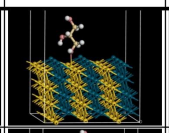	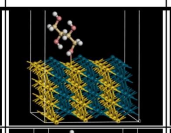	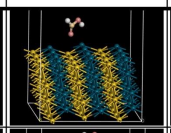	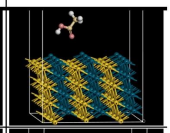
AuPd*@C (111)	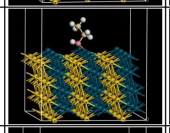	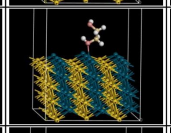	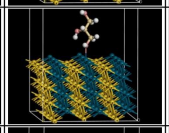	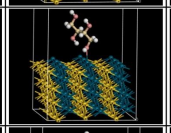	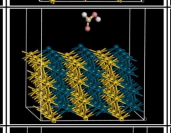	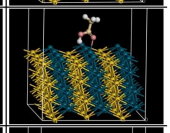
Au*Pd@C (200)	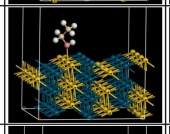	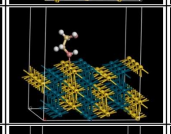	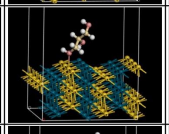	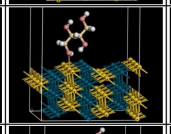	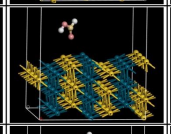	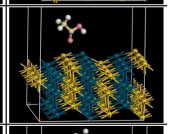
AuPd*@C (200)	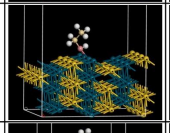	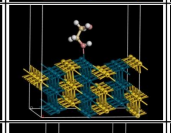	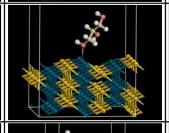	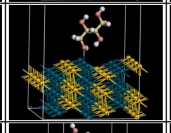	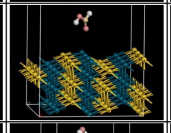	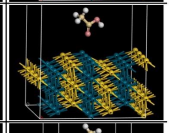
Au*@C(111)	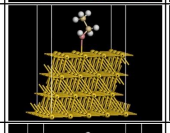	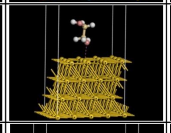	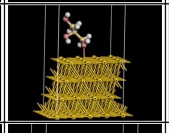	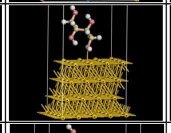	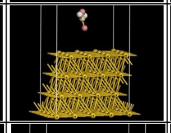	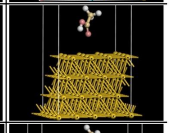
Au*@C (200)	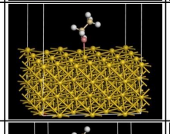	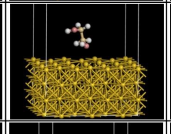	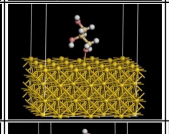	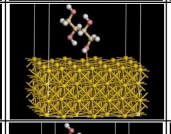	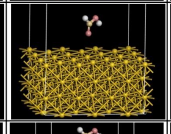	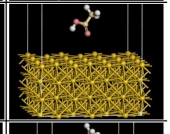
Pd*@C(111)	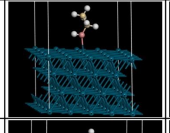	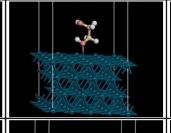	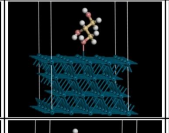	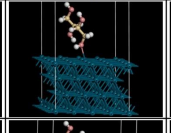		
Pd*@C (200)						
Pt*@C(111)						
Pt*@C (200)						

Fig. S7. The optimized structures of adsorption of ethanol, glycol, glycerin and erythritol and desorption of formic acid and acetic acid on all kinds of metal sites of as-prepared model catalysts, respectively.

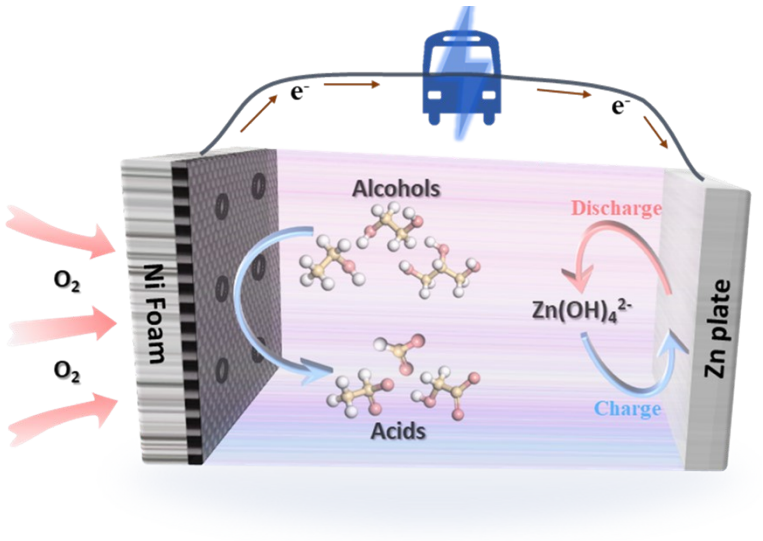

Fig. S8. Schematic diagram of zinc-alcohol-air batteries.

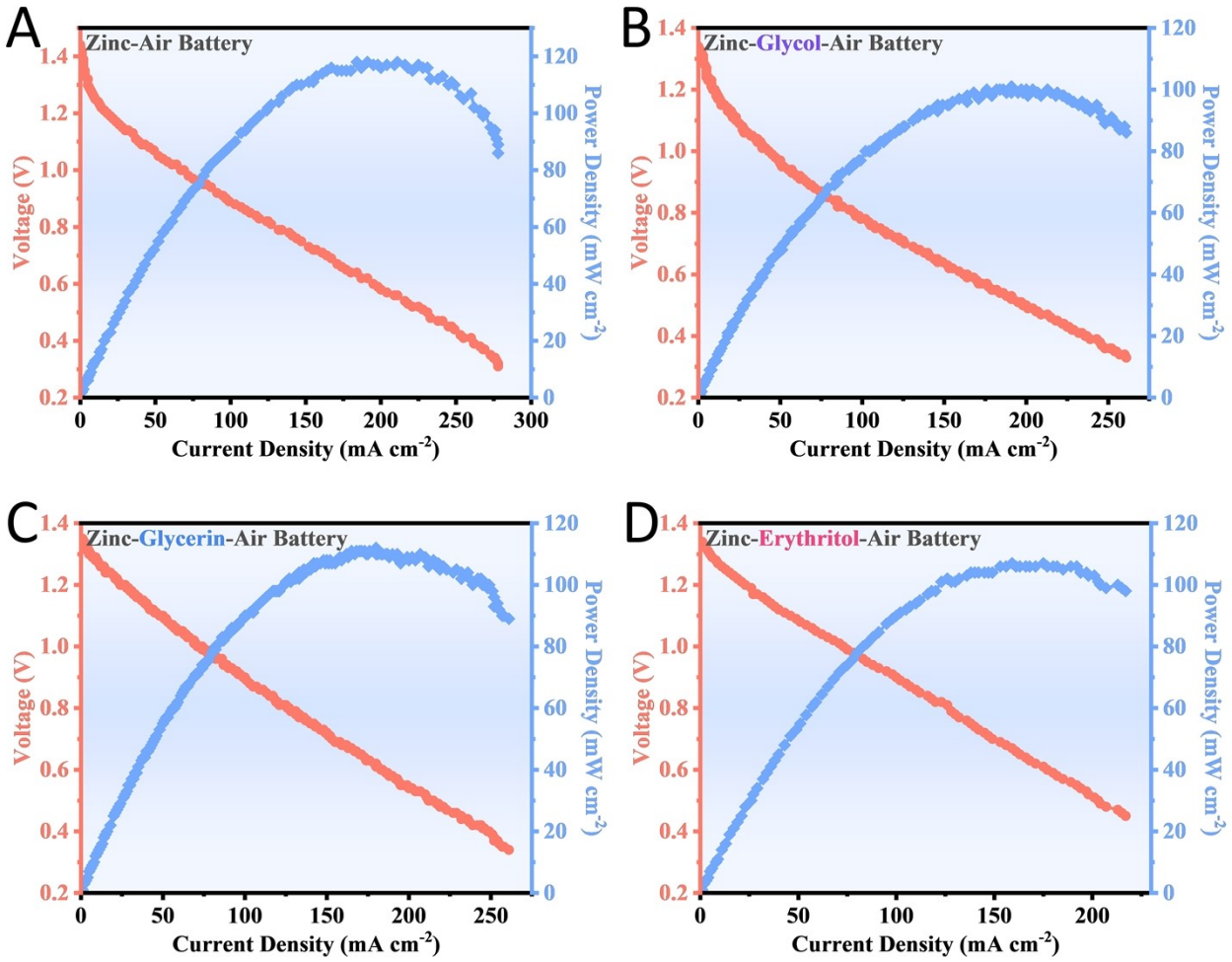

Fig. S9. (A-F) Discharging and power density curves for zinc-air battery, zinc-glycol-air battery, zinc-glycerin-air battery and zinc-erythritol-air battery, respectively.

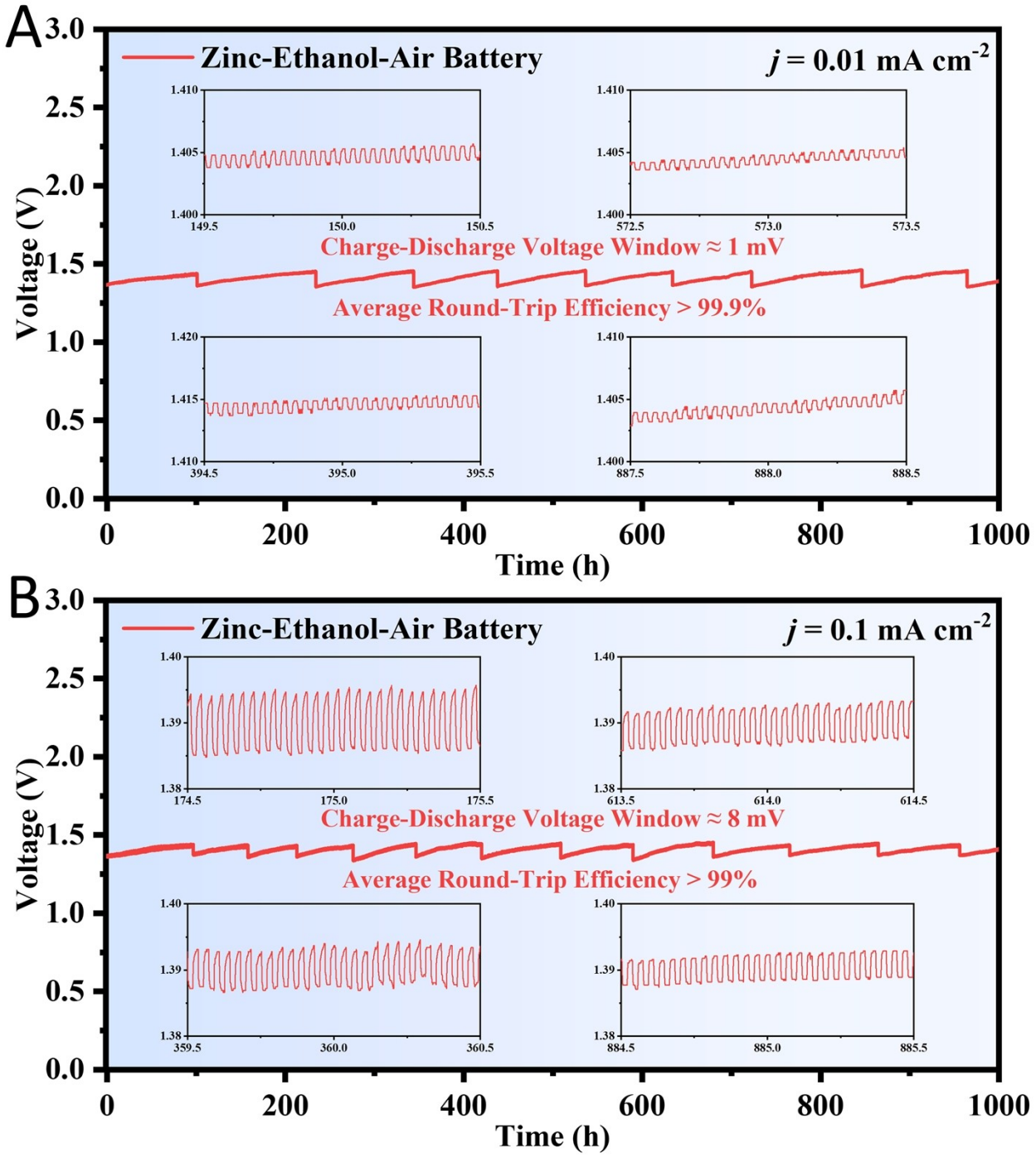

Fig. S10. (A, B) Long-term cyclic stability profiles of zinc-ethanol-air battery at the current density of 0.01 and 0.1 mA cm^{-2}, respectively.

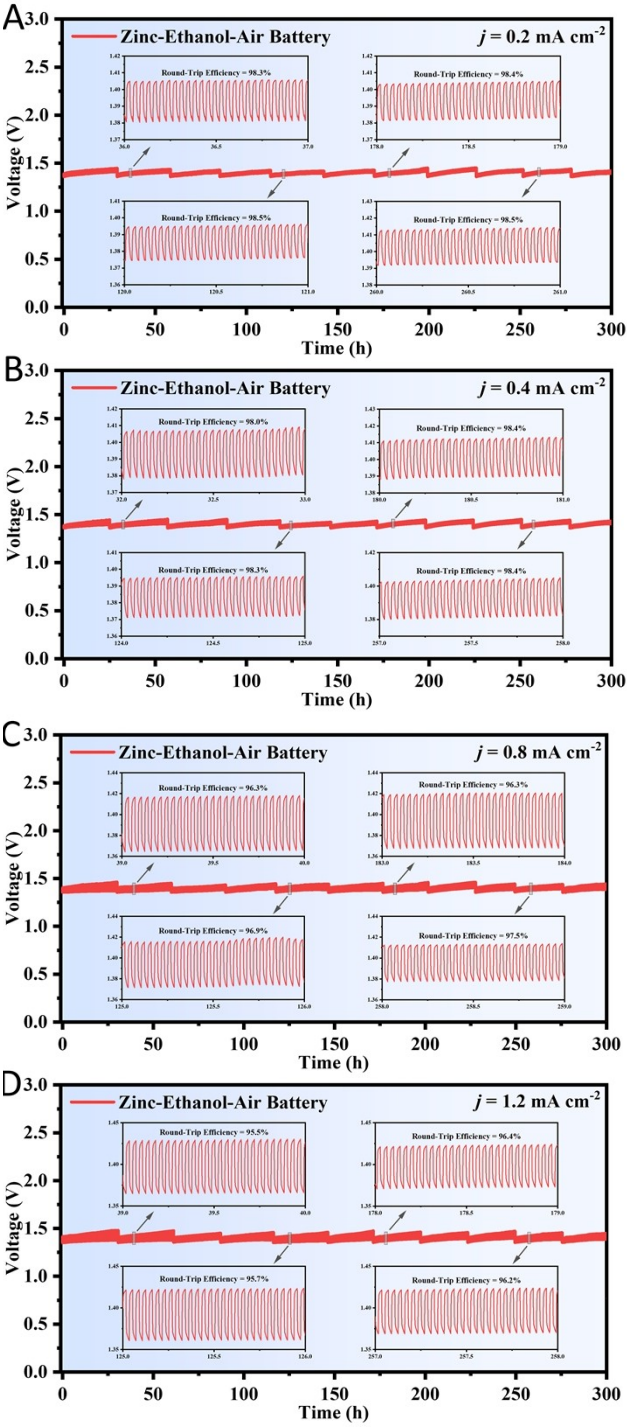

Fig. S11. (A-D) Long-term cyclic stability profiles of zinc-ethanol-air battery at the current density of 0.2, 0.4, 0.8 and 1.2 mA cm^{-2}, respectively.

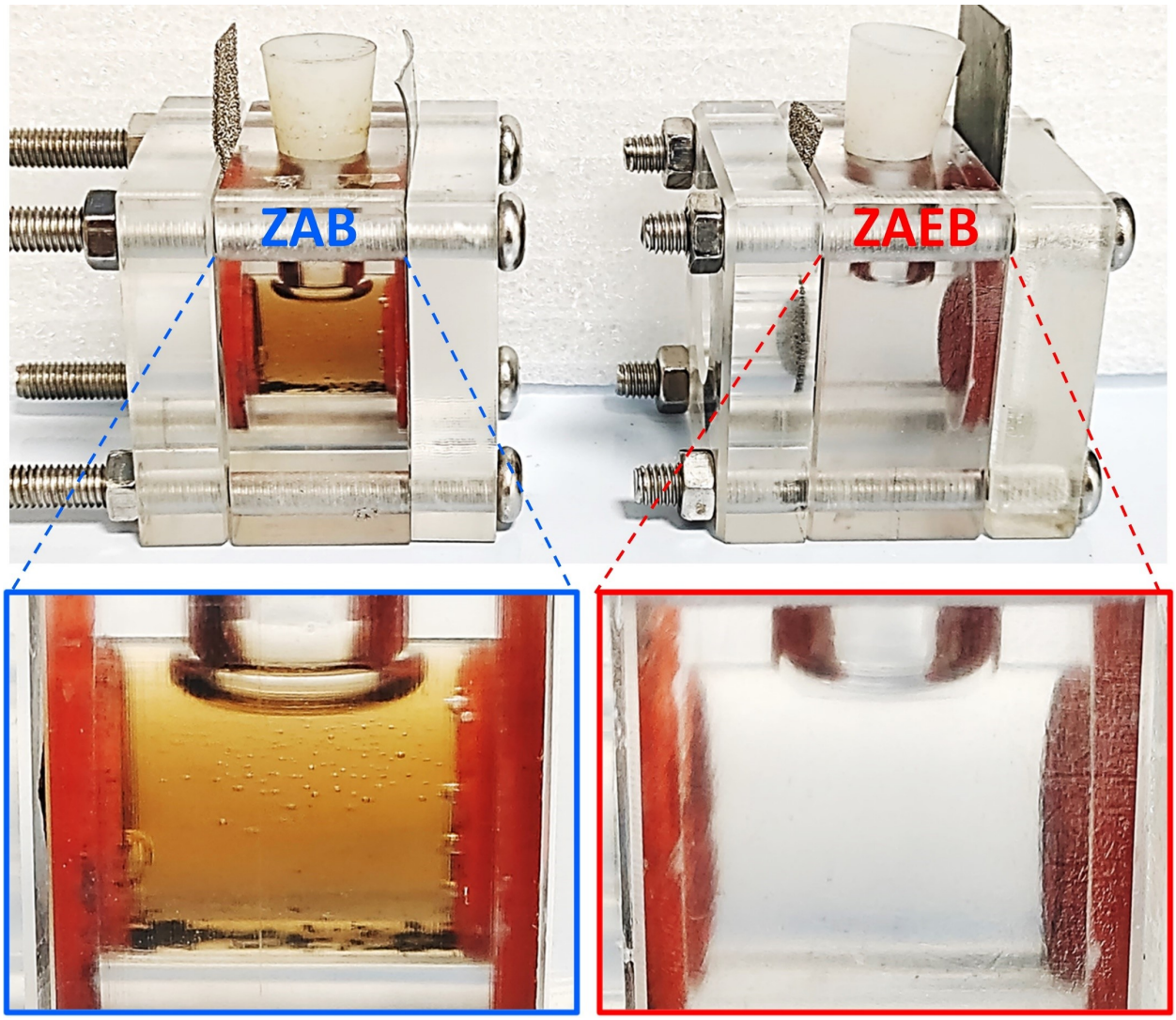

Fig. S12. Photographs of zinc-air battery and zinc-ethanol-air battery after 20 h cyclic tests at the current density of 2 mA cm^{-2}.

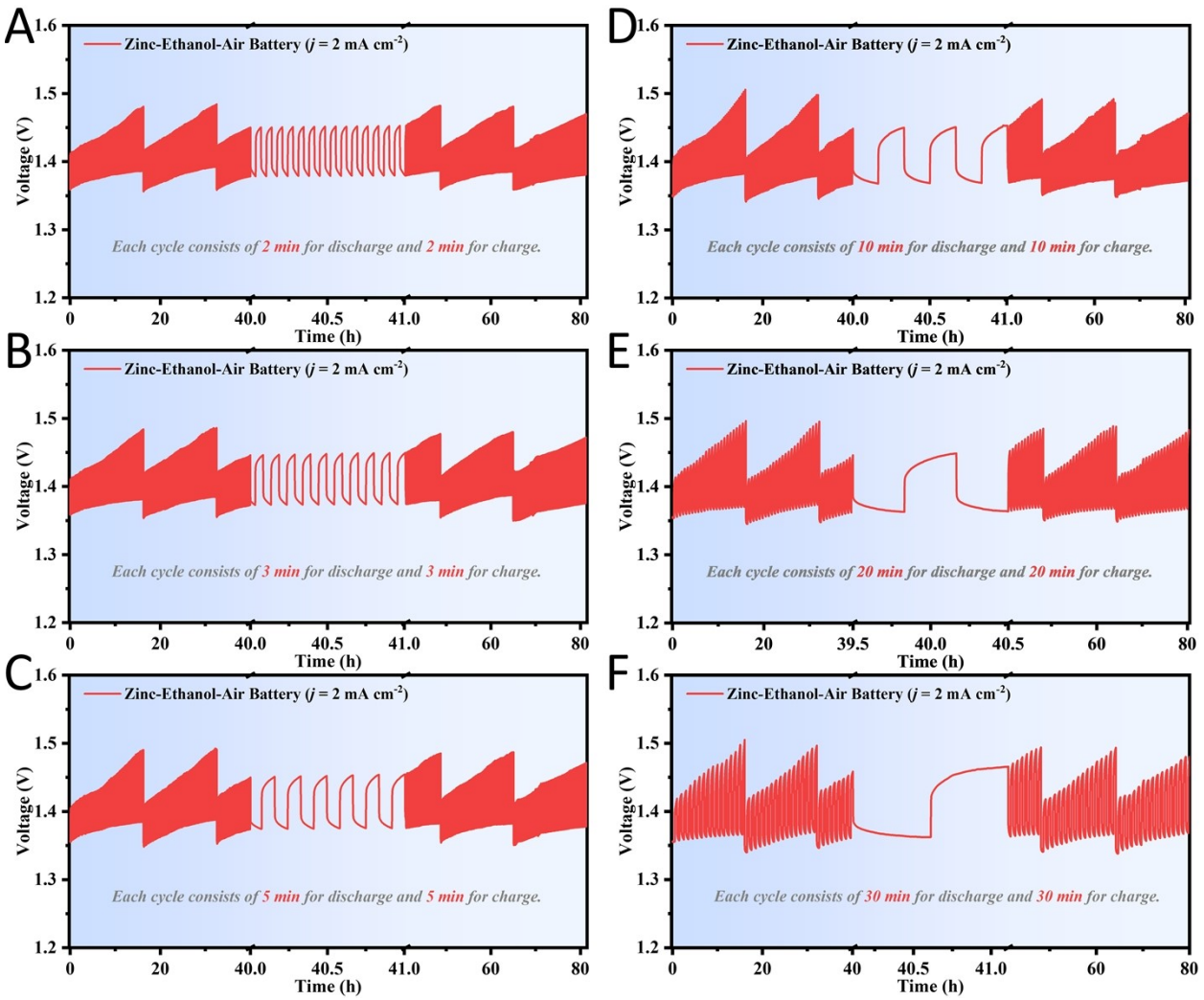

Fig. S13. Cyclic performance profiles at the current density of 2.0 mA cm^{-2} with 15, 10, 6, 3, 2, 1 cycle per hour.

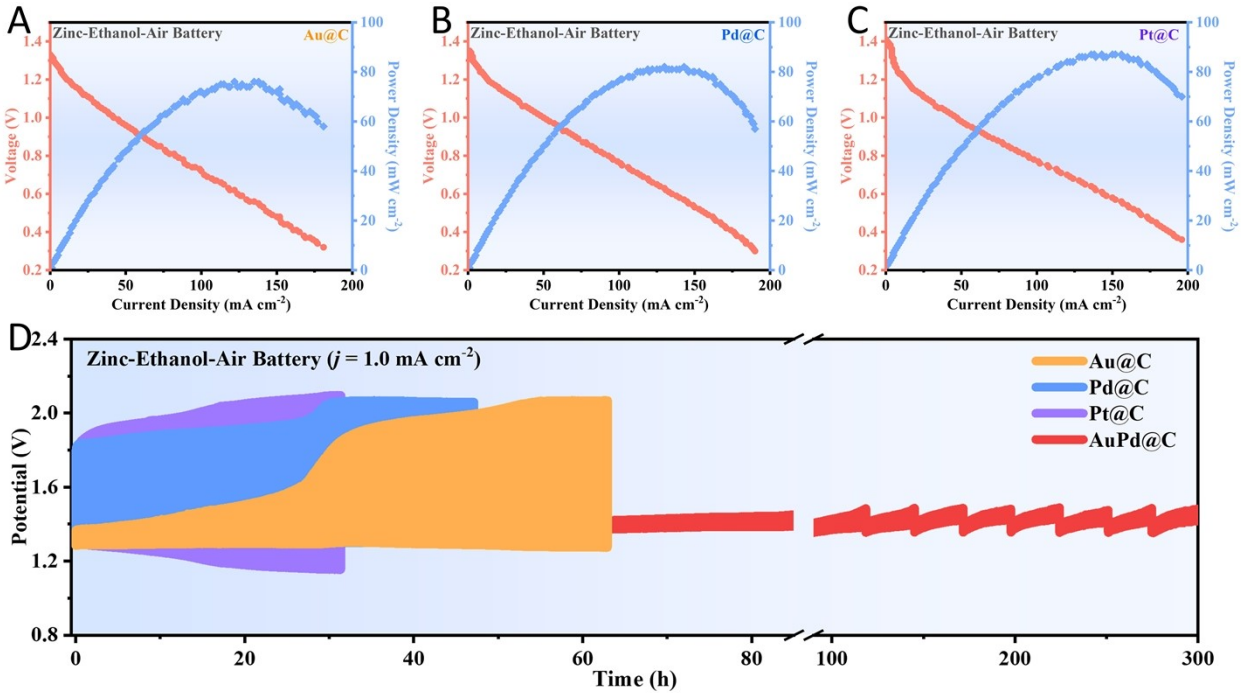

Fig. S14. (A-C) Discharging and power density curves of Au@C, Pd@C and Pt@C for zinc-ethanol-air battery. (D) Cyclic performance profiles of Au@C, Pd@C, Pt@C and AuPd@C for zinc-ethanol-air battery at the current density of 1.0 mA cm^{-2}.

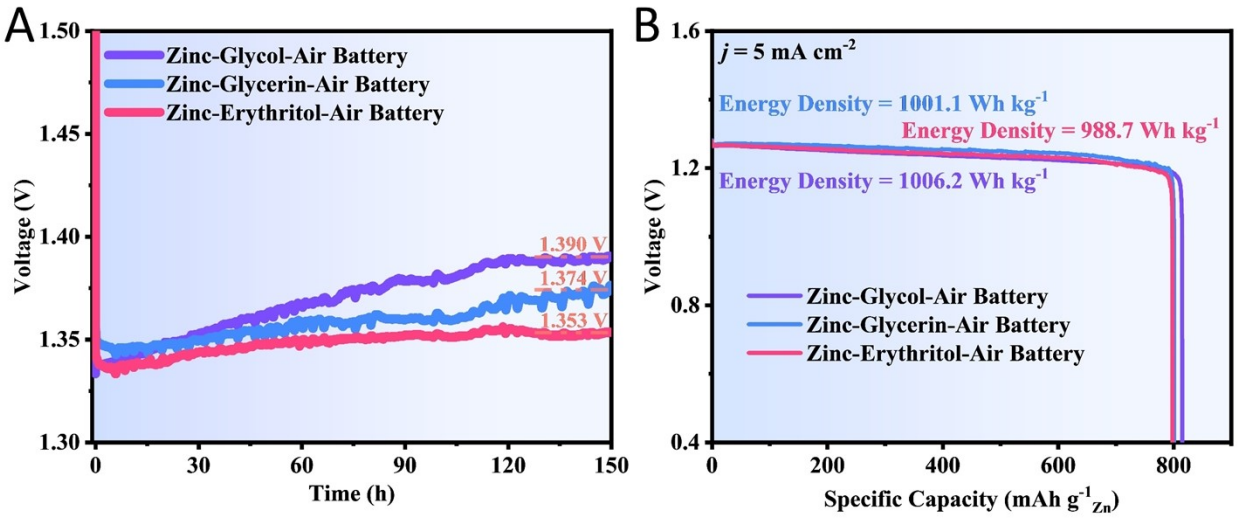

Fig. S15. (A) OCV plots and (B) discharging capacity curves of zinc-glycol-air battery, zinc-glycerin-air battery and zinc-erythritol-air battery.

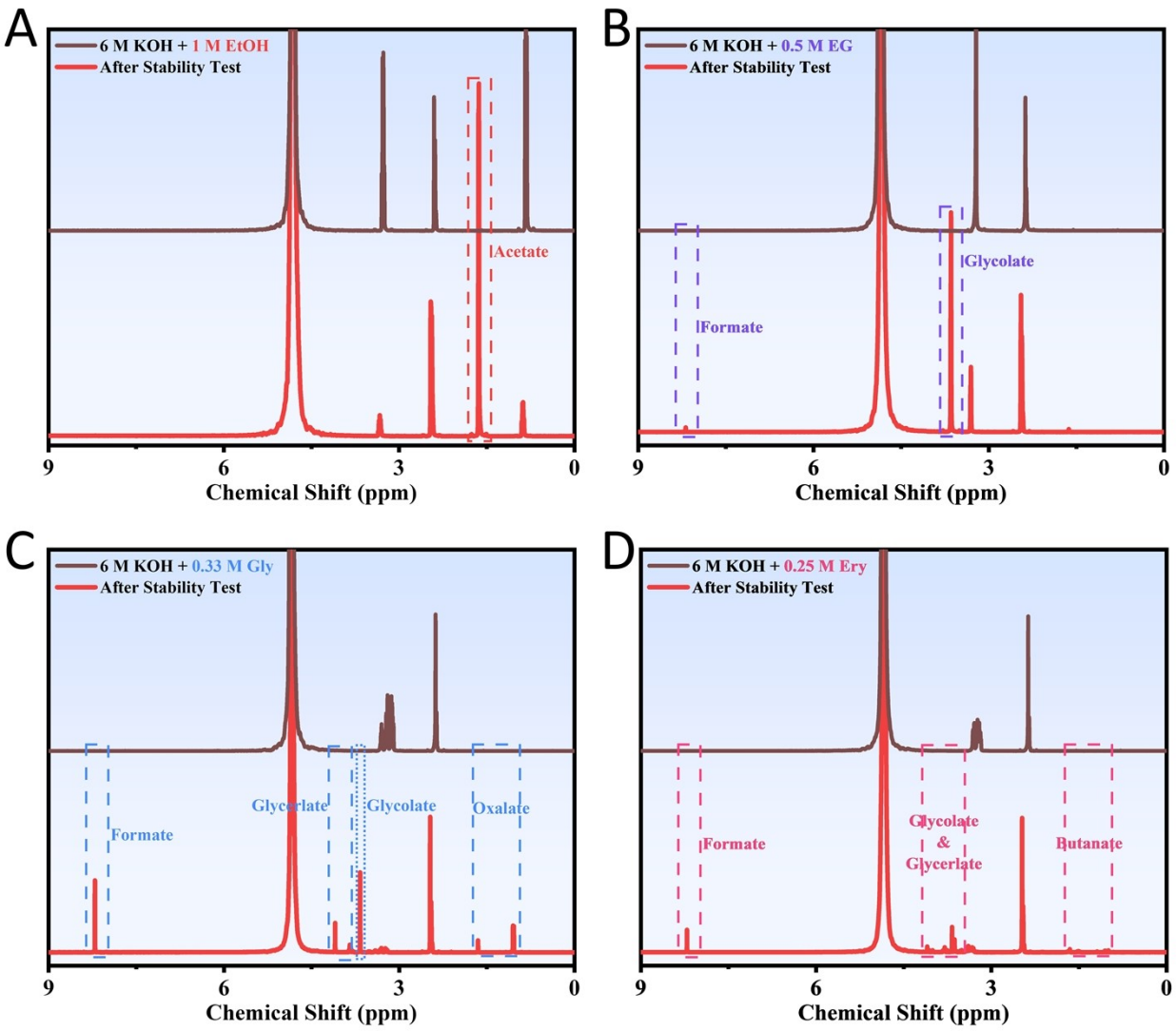

Fig. S16. (A-F) ^{1}H NMR spectra of products before and after cyclic stability test for zinc-ethanol-air battery, zinc-glycol-air battery, zinc-glycerin-air battery and zinc-erythritol-air battery, respectively.

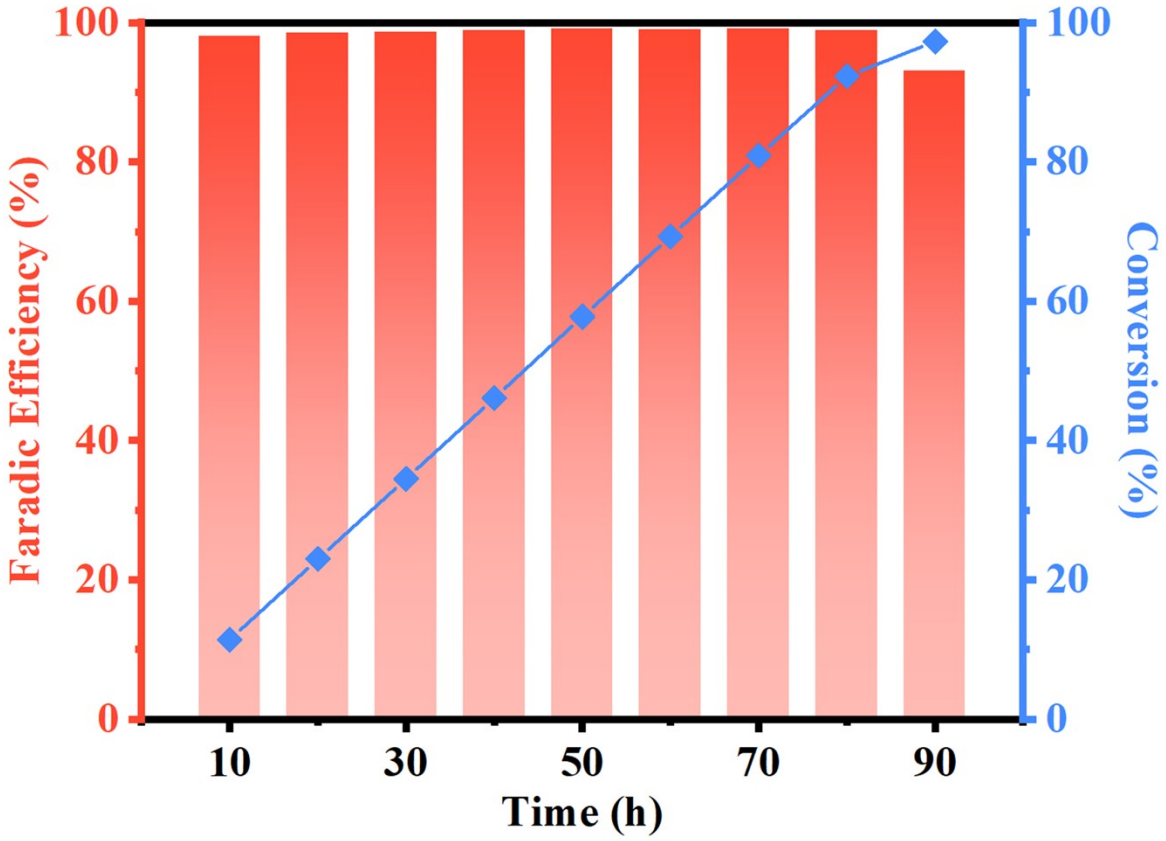

Fig. S17. Time-dependent Faradaic efficiency and conversion curves of the $4e^-$ EOR catalyzed by AuPd@C. The electrolyte without refreshing was collected every 10 hours during the cyclic test and analyzed using ^1H NMR.

Fig. S18. Photograph of the AuPd@C catalyst obtained in the scale-up production. The raw material of single synthesis includes 1.0 g of $HAuCl_4 \cdot 3H_2O$, 0.5 g of $PdCl_2$ and 7.95 g of Ketjen black (carbon support).

Supplementary Tables

Table S1. Fitting data for XRD.

Peak (°)	Ketjen Black	Au@C		Pd@C		Pt@C		AuPd@C			
2θ-Range	5.1°-74.8°	5.1°-74.8°		6.2°-73.8°		5.7°-73.5°		6.7°-73.5°			
Carbon 1	8.38°	6.94°		8.35°		8.24°		9.03°			
Carbon 2	24.08° (002)	24.05° (002)		23.77° (002)		23.69° (002)		23.72° (002)			
Carbon 3	43.82° (101)	42.67° (101)		43.12° (101)		43.64° (101)		42.63° (101)			
Fitting Results	-	**2θ**	**FWHM**	**2θ**	**FWHM**	**2θ**	**FWHM**	**Au:2θ**	**FWHM**	**Pd:2θ**	**FWHM**
Metal 1	-	38.06°	2.08°	39.9°	1.33°	39.69°	2.83°	38.44°	1.92°	39.10°	1.93°
Metal 2	-	44.21°	2.55°	46.30°	1.74°	46.19°	3.29°	44.65°	2.32°	45.87°	2.38°
Metal 3	-	64.60°	2.65°	68.10°	2.02°	67.77°	3.50°	65.21°	2.53°	66.75°	2.57°
Crystallite Size	-	3.81 nm		5.51 nm		2.91 nm		4.12 nm		4.08 nm	

Table S2. The ratio of elements obtained by XPS.

Samples	Au (Atomic %)	Pd (Atomic %)	O (Atomic %)
Au@C	0.44	-	1.43
Pd@C	-	0.74	1.34
AuPd@C	0.39	0.36	0.62

Table S3. The contents of Au and Pd are obtained in different ways.

Elements	at% (Input)	wt% (Input)	at% (XPS)	wt% (XPS)	at% (ICP)	wt% (ICP)
Au	0.38	5.7	0.39	5.9	0.37	5.6
Pd	0.41	3.4	0.36	2.9	0.38	3.0

Table S4. The adsorption energy of ethanol, glycol, glycerin and erythritol and the desorption energy of formic acid and acetic acid for all kinds of metal sites of as-prepared model catalysts, respectively.

*represent adsorbate	Adsorption Energy (eV)				Desorption Energy (eV)	
	Ethanol	Glycol	Glycerin	Erythritol	Formic Acid	Acetic Acid
Au*Pd@C (111)	-1.90	-1.75	-1.97	-1.67	1.51	1.48
AuPd*@C (111)	-1.90	-1.81	-1.97	-1.88	2.14	1.51
Au*Pd@C (200)	-1.21	-1.18	-1.31	-1.16	1.24	1.20
AuPd*@C (200)	-1.59	-1.47	-1.64	-1.62	1.78	1.23
Au*@C(111)	-1.47	-1.39	-1.49	-1.44	1.47	1.38
Au*@C (200)	-1.61	-1.54	-1.58	-1.61	1.58	1.52
Pd*@C(111)	-1.39	-1.25	-1.43	-1.37	1.22	1.13
Pd*@C (200)	-1.45	-1.34	-1.44	-1.43	1.22	1.18
Pt*@C(111)	-1.45	-1.25	-1.5	-1.39	1.64	1.20
Pt*@C (200)	-1.66	-1.52	-1.74	-1.60	1.42	1.38

Table S5. Performance statistics of some state-of-the-art zinc-air batteries recently.

Battery	Long-term cycling Window	RTE	Durability	Reference
ZEAB	1 mV @ 0.01 mA cm^{-2}	**99.9%**	**1000 h**	This Work
ZEAB	8 mV @ 0.1 mA cm^{-2}	**99%**	**1000 h**	This Work
ZEAB	80 mV @ 2.0 mA cm^{-2}	**94%**	**1000 h**	This Work
ZAB	810 mV @ 10 mA cm^{-2}	**58.5%**	**200 h**	Ref.44
Neutral ZAB	1280 mV @ 0.2 mA cm^{-2}	**61%**	**400 h**	Ref.41
ZAB	770 mV @ 10 mA cm^{-2}	**62.5%**	**600 h**	Ref.45
ZAB	900 mV @ 2.0 mA cm^{-2}	**55%**	**1600 h**	Ref.46
ZAB	950 mV @ 10 mA cm^{-2}	**53%**	**720 h**	Ref.47
ZAB	900 mV @ 2.0 mA cm^{-2}	**57%**	**200 h**	Ref.48
Zn-NO_3^-/EtOH Batteries	680 mV @ 0.1 mA cm^{-2}	**64%**	**40 h**	Ref.13
All-temperature ZAB	750 mV @ 0.4 mA cm^{-2}	**57%**	**800 h**	Ref.8
ZAB	700 mV @ 2.0 mA cm^{-2}	**65%**	**160 h**	Ref.49
ZEAB	800 mV @ 10 mA cm^{-2}	**60%**	**108 h**	Ref.12
ZAB with PILG	850 mV @ 0.5 mA cm^{-2}	**62%**	**1000 h**	Ref.50
ZAB (Zn-O_2/ZnO_2)	800 mV @ 0.1 mA cm^{-2}	**54%**	**1600 h**	Ref.6
ZAB (Zn-O_2/ZnO_2)	1250 mV @ 1.0 mA cm^{-2}	**39%**	**160 h**	Ref.6
Zinc-Air Pouch Cells	700 mV @ 25 mA cm^{-2}	**64.1%**	**800 h**	Ref.9
ZAB	720 mV @ 10 mA cm^{-2}	**62%**	**500 h**	Ref.51
Light-Assisted ZAB	390 mV @ 0.5 mA cm^{-2}	**70.3%**	**50 h**	Ref.52

Table S6. Properties of zinc-ethanol-air battery compared with zinc-air battery and direct ethanol fuel cell. The loading of noble metals in the electrode is 0.1 mg cm^{-1}.

Properties	Zinc-Air Battery	Zinc-Ethanol-Air Battery	Direct Ethanol Fuel Cell
OCV (Virtual OCV)	1.65 V (1.48 V)	1.65 V (1.49 V)	1.14 V (1.0 V)
Operating Temperature	R.T.	R.T.	60-90 °C
Start-Up Time	Immediate	Immediate	Seconds to Minutes
Power Density (With O_2)	120 mW cm^{-2} (190 mW cm^{-2})	110 mW cm^{-2} (180 mW cm^{-2})	50 mW cm^{-2} (120 mW cm^{-2})
Energy Density	~990 Wh kg^{-1}	~1020 Wh kg^{-1}	~2000 Wh L^{-1}
Cyclic Voltage Window	700 mV @ 2 mA cm^{-2}	80 mV @ 2 mA cm^{-2}	-
Initial Discharging Voltage	~1.4 V	~1.35 V	~0.9 V
Discharging Efficiency	~75%	~75%	~30%
Charge Efficiency	~60%	>90%	-
Overall Efficiency	~45%	~70%	~30%
Positive Reaction	OER & ORR	EOR & ORR	EOR
Gas Generation	O_2	none	CO_2/CO
Stability Time	~500 h	>1000 h	<100 h
Electrolyte	6 M KOH	6 M KOH + 1 M EtOH	1 M KOH + 2 M EtOH